

# Spatial correlations in chaotic nanoscale systems with spin-orbit coupling

Anh T. Ngo,<sup>1</sup> Eugene H. Kim,<sup>2,3</sup> and Sergio E. Ulloa<sup>1</sup>

<sup>1</sup>*Department of Physics and Astronomy, and Nanoscale & Quantum Phenomena Institute, Ohio University, Athens, Ohio 45701*

<sup>2</sup>*Instituto de Física Teórica, UAM-CSIC, Madrid 28049, Spain*

<sup>3</sup>*Department of Physics, University of Windsor, Windsor, Ontario, Canada N9B 3P4*

We investigate the statistical properties of wave functions in chaotic nanostructures with spin-orbit coupling (SOC), focussing in particular on spatial correlations of eigenfunctions. Numerical results from a microscopic model are compared with results from random matrix theory in the crossover from the gaussian orthogonal to the gaussian symplectic ensembles (with increasing SOC); one- and two-point distribution functions were computed to understand the properties of eigenfunctions in this crossover. It is found that correlations of wave function amplitudes are suppressed with SOC; nevertheless, eigenfunction correlations play a more important role in the two-point distribution function(s), compared to the case with vanishing SOC. Experimental consequences of our results are discussed.

PACS numbers: 71.70.Ej, 73.63.-b, 73.63.Kv

## I. INTRODUCTION

Spin-orbit coupling (SOC) has the potential to make novel electronics applications possible,<sup>1</sup> as it allows one to control the electron's spin degree of freedom through its motion. Most systems of interest for such applications are nano- or mesoscopic in size, including semiconductor quantum dots,<sup>2</sup> metallic nanoparticles,<sup>3</sup> and quantum corrals defined on surfaces.<sup>4</sup> The energy spectrum, and more generally, properties of these systems are (typically) described by random matrix theory (RMT).<sup>5,6</sup>

In RMT, the system's properties are a consequence of its symmetries — in the classic Wigner-Dyson ensembles, the key symmetries are time-reversal ( $T$ ) and spin-rotation ( $\sigma$ ) invariance.<sup>5,6</sup> With both  $T$ - and  $\sigma$ -invariance, the system is described by the gaussian orthogonal ensemble (GOE); SOC breaks the  $\sigma$ -invariance (while preserving  $T$ -invariance), driving the system to the gaussian symplectic ensemble (GSE). [Systems with broken  $T$ -invariance are described by the gaussian unitary ensemble (GUE).] More specifically, systems with SOC are described by random  $N \times N$  matrices (with  $N \rightarrow \infty$ ) having quaternion components

$$H = S \otimes I_2 + i \frac{\lambda}{\sqrt{4N}} \sum_{j=1}^3 A_j \otimes \sigma^j, \quad (1)$$

where  $S$  is an  $N \times N$  symmetric matrix, and the  $\{A_j\}$  are  $N \times N$  antisymmetric matrices;  $\{\sigma^j\}$  are the Pauli matrices, and  $I_2$  is the  $2 \times 2$  identity matrix.  $\lambda$  in Eq. 1 is related to the SOC of the microscopic Hamiltonian —  $\lambda=0$  in the GOE, while  $\lambda=\sqrt{4N}$  in the GSE.

As most nanoscale systems of interest are described by RMT,<sup>2-6</sup> it is important to understand the regimes/behaviors which arise with SOC and the properties in these regimes. In this work, we consider the spatial properties of wave functions in (two-dimensional) chaotic nanoscale systems with SOC. The spatial properties of wave functions often determine the system's response to experimental probes, and are important for devices/applications.<sup>7-14</sup> While other works have dis-

cussed properties/consequences of eigenvector statistics with SOC,<sup>15,16</sup> here we consider the spatial properties of eigenvectors and, in particular, how these properties evolve with the SOC.

In what follows, we consider the properties of the Hamiltonian

$$H = \frac{1}{2m} \mathbf{p}^2 + \alpha \hat{z} \cdot (\mathbf{p} \times \vec{\sigma}) + V(\mathbf{r}), \quad (2)$$

where  $V(\mathbf{r})$  is a confining and/or disorder potential. Results obtained via RMT are compared with those obtained by direct simulation of Eq. 2 for a stadium billiard.<sup>17</sup> To characterize the system and understand its properties, one- and two-point distribution functions were computed in the crossover from the GOE to the GSE (with increasing SOC). In particular, it is found that excellent agreement between RMT and microscopic simulations are obtained in a “mean-field” description of the (GOE-GSE) crossover (see below). A key observation from our results is that correlations of wave function amplitudes are suppressed with SOC. Interestingly, however, these correlations play a more important role in the two-point distribution function(s), compared to the GOE (with vanishing SOC).

The rest of the paper is organized as follows. The description of wave function statistics in RMT and, in particular, the description of the GOE-GSE crossover is discussed in Sec. II. Details of our microscopic calculations — namely the stadium billiard considered as well as the numerical approach employed — are presented in Sec. III. Our results are presented in Sec. IV — one- and two-point distribution functions obtained via RMT are compared with numerical results from the stadium billiard. Finally, Sec. V contains a summary of our results as well as remarks on experimental consequences.

## II. WAVE FUNCTION STATISTICS IN RMT

In RMT, wave function correlations are governed by the functional probability distribution<sup>18,19</sup>

$$\mathcal{P}(\psi) = \mathcal{N} \exp \left[ -\frac{\beta}{2} \sum_{s,s'} \int d\mathbf{r} d\mathbf{r}' \psi_s^*(\mathbf{r}) K_{s,s'}(\mathbf{r}, \mathbf{r}') \psi_{s'}(\mathbf{r}') \right]. \quad (3)$$

$K_{s,s'}(\mathbf{r}, \mathbf{r}')$  is the functional inverse of the two-point correlation function  $\langle \psi_s^*(\mathbf{r}) \psi_{s'}(\mathbf{r}') \rangle$ , where the angular brackets  $\langle \dots \rangle$  denote an average with respect to  $\mathcal{P}(\psi)$ ; the parameter  $\beta$  depends on the system's symmetries —  $\beta=1$  ( $\beta=2$ ) in the GOE (GUE), while  $\beta=4$  in the GSE. [ $\mathcal{N}$  is a normalization constant.]  $\mathcal{P}(\psi)$  is the probability that a particular energy eigenfunction with spin- $\sigma$  is equal to the specified function  $\psi_\sigma(\mathbf{r})$ .

A key property of Eqs. 1 and 2 is their invariance under time-reversal; as a result, the energy levels are two-fold degenerate — the eigenstates  $\{\psi(\mathbf{r}), \mathcal{T}\psi(\mathbf{r})\}$  are degenerate, where  $\mathcal{T}$  is the time-reversal operator. Explicitly,

$$\psi(\mathbf{r}) = \begin{pmatrix} \phi(\mathbf{r}) \\ \chi(\mathbf{r}) \end{pmatrix}, \quad \mathcal{T}\psi(\mathbf{r}) = \begin{pmatrix} -\chi^*(\mathbf{r}) \\ \phi^*(\mathbf{r}) \end{pmatrix}. \quad (4)$$

As a consequence of this two-fold degeneracy, the wave function amplitude probed numerically and experimentally is  $|\psi_\sigma(\mathbf{r})|^2 = |\phi(\mathbf{r})|^2 + |\chi(\mathbf{r})|^2$ . As noted above, we are interested in the regimes/behaviors which arise with SOC — we will not only be interested in the GSE, but also in the crossover from the GOE to the GSE. As such, we decompose the complex wave functions  $\phi(\mathbf{r})$  and  $\chi(\mathbf{r})$  in Eq. 4 into their real and imaginary parts. Then, the wave function amplitude is parameterized as

$$|\psi_\sigma(\mathbf{r})|^2 = \gamma_1^2 \phi_1^2(\mathbf{r}) + \gamma_2^2 \phi_2^2(\mathbf{r}) + \gamma_3^2 \chi_1^2(\mathbf{r}) + \gamma_4^2 \chi_2^2(\mathbf{r}), \quad (5)$$

where the parameters  $\{\gamma_i\}$ , which satisfy the constraint  $\gamma_1^2 + \gamma_2^2 + \gamma_3^2 + \gamma_4^2 = 1$ , characterize the crossover —  $\gamma_1=1$  with  $\gamma_i=0$  for  $i \neq 1$  in the GOE, while  $\gamma_i=1/2$  ( $i = 1 \dots 4$ ) in the GSE; in the crossover, the  $\{\gamma_i\}$  fluctuate and, hence, physical quantities must be averaged over their distribution.

We obtained  $\mathcal{P}(\{\gamma_i\})$ , the distribution of the  $\{\gamma_i\}$ , numerically from Eq. 1 by considering the various orthogonal invariants<sup>20</sup> — the results are shown in Fig. 1. We see that the  $\mathcal{P}(\{\gamma_i\})$  change rapidly for  $\lambda/\sqrt{4N} \lesssim 0.1$  — in particular, the  $\mathcal{P}(\{\gamma_i\})$  are broad for small  $\lambda$ , but become sharply peaked gaussian-like for larger values of  $\lambda$ , moving towards  $\gamma_i=1/2$  ( $\forall i$ ) with increasing  $\lambda$ . Figure 2 shows the variance of the  $\{\gamma_i\}$ ,  $\langle \gamma_i^2 \rangle - \langle \gamma_i \rangle^2$ , as a function of  $\lambda$ ; the inset shows how the average values of the  $\{\gamma_i\}$ ,  $\langle \gamma_i \rangle$ , evolve with  $\lambda$ . We see that the variance is extremely small for larger values of  $\lambda$ ; even for small values of  $\lambda$  (where the  $\mathcal{P}(\{\gamma_i\})$  are broad and asymmetric), the variance does not exceed 0.03. As noted above, physical quantities must be averaged over the  $\mathcal{P}(\{\gamma_i\})$ ; however, as will be seen below, rather good results are obtained in a “mean-field” description (due to the small variances), similar to what has been observed in the GOE-GUE

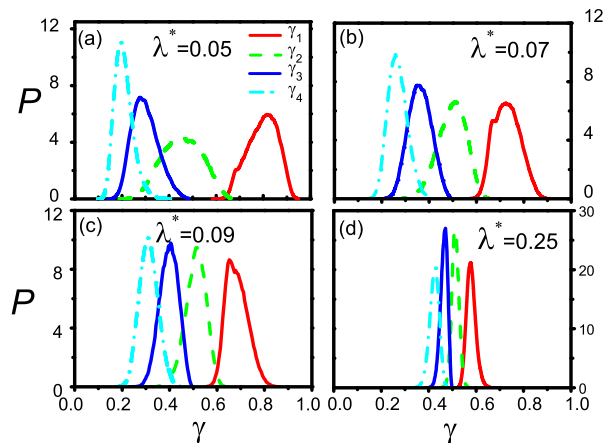


FIG. 1: (color online) Distribution of the  $\{\gamma_i\}$ ,  $\mathcal{P}(\{\gamma_i\})$  (from Eq. 5), where  $\lambda^* = \lambda\sqrt{4N}$ . (a)  $\lambda^* = 0.05$  (b)  $\lambda^* = 0.07$  (c)  $\lambda^* = 0.09$  (d)  $\lambda^* = 0.25$ . Notice all  $\mathcal{P}$  change rapidly for  $\lambda^* \lesssim 0.1$  and become sharply peaked at  $\gamma \simeq 1/2$  for large  $\lambda^*$ .

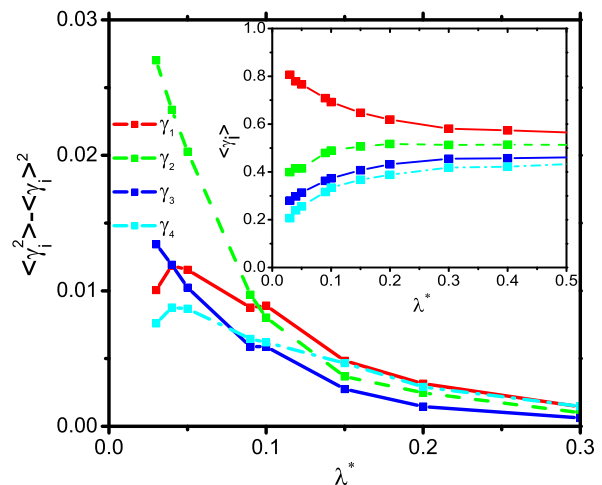


FIG. 2: (color online) Variance of  $\{\gamma_i\}$  vs.  $\lambda^* = \lambda\sqrt{4N}$ . Inset: average values of  $\{\gamma_i\}$  vs.  $\lambda^*$ .

crossover<sup>10,21</sup> — rather good results are obtained by approximating the  $\{\gamma_i\}$  by their average values (rather than averaging over the  $\mathcal{P}(\{\gamma_i\})$ ).

From Eq. 3, all spatial correlations can be obtained once the two-point correlation function  $\langle \psi_s^*(\mathbf{r}) \psi_{s'}(\mathbf{r}') \rangle$  is known. To determine this, we expand the wave function as

$$\psi(\mathbf{r}) = \sum_{\mathbf{p}} \psi_{+,\mathbf{p}}(\mathbf{r}) c_{+,\mathbf{p}} + \psi_{-,\mathbf{p}}(\mathbf{r}) c_{-,\mathbf{p}}, \quad (6)$$

where the two-component spinors  $\psi_{+,\mathbf{p}}(\mathbf{r})$  and  $\psi_{-,\mathbf{p}}(\mathbf{r})$  are eigenstates of Eq. 2 with  $V(\mathbf{r}) = 0$ . Explicitly, the eigenvalues  $\{E_+, E_-\}$  and corresponding eigenstates

$\{\psi_{+,\mathbf{p}}(\mathbf{r}), \psi_{-,\mathbf{p}}(\mathbf{r})\}$  are ( $\hbar = 1$ )

$$E_{\pm} = \frac{|z|^2}{2m} \pm \alpha|z|; \quad \psi_{\pm,\mathbf{p}}(\mathbf{r}) = \frac{1}{\sqrt{2A}} \begin{pmatrix} 1 \\ \pm iz/|z| \end{pmatrix} e^{i\mathbf{p}\cdot\mathbf{r}}$$

where  $z=p_x+ip_y$ . The spectrum above describes two spin-split chiral surfaces with energy  $E$ , shown schematically in Fig. 3a, where  $k_{\pm} = \sqrt{2mE + m^2\alpha^2} \mp m\alpha$ .

To compute  $\langle \psi_s^*(\mathbf{r}) \psi_{s'}(\mathbf{r}') \rangle$ , the Fourier coefficients (in Eq. 6) are taken to be gaussian random variables having zero mean and variance given by<sup>8</sup> ( $a,b=+,-$ )

$$\langle c_{a,\mathbf{p}}^* c_{b,\mathbf{k}} \rangle = \delta_{a,b} \delta_{\mathbf{p},\mathbf{k}} \frac{1}{N(\epsilon)} \delta(\epsilon(\mathbf{p}) - \epsilon), \quad \langle c_{a,\mathbf{p}} c_{b,\mathbf{k}} \rangle = 0. \quad (7)$$

Writing the wave function as per Eq. 4 and using the parameterization in Eq. 5, we obtain<sup>22</sup> ( $i,j=1,2$ )

$$\langle \phi_i(\mathbf{r}) \phi_j(\mathbf{r}') \rangle = \langle \chi_i(\mathbf{r}) \chi_j(\mathbf{r}') \rangle = \delta_{i,j} f, \quad (8a)$$

$$\langle \phi_i(\mathbf{r}) \chi_j(\mathbf{r}') \rangle = -\langle \chi_i(\mathbf{r}) \phi_j(\mathbf{r}') \rangle = \delta_{i,j} g, \quad (8b)$$

where

$$f = \frac{1}{2} [J_0(k_+R) + J_0(k_-R)], \quad (9a)$$

$$g = \frac{1}{2} [J_1(k_+R) - J_1(k_-R)]. \quad (9b)$$

In Eqs. 9a and 9b,  $J_0(x)$  ( $J_1(x)$ ) is the Bessel function of order-0 (order-1),<sup>23</sup>  $R=|\mathbf{r} - \mathbf{r}'|$ , and  $k_{\pm}$  are the wave vectors associated with the chiral branches at energy  $E$ . The physics of Eq. 7 (and Eqs. 8a and 8b) is that the system ergodically samples the energy surfaces<sup>24</sup> (shown schematically in Fig. 3a).

### III. NUMERICS

As described above, we are interested in comparing results obtained via RMT with those obtained by direct simulation of Eq. 2. To this end, we have computed the local density of states (LDOS) for a stadium billiard,<sup>17</sup> where the billiard's wall was constructed with a unitary delta-function potential<sup>25</sup>

$$V(\mathbf{r}) = V_0 \delta(\mathbf{r} - \mathbf{R}(s)), \quad (10)$$

with  $\mathbf{R}(s)$  parameterizing the wall (and  $V_0 \rightarrow \infty$ ). The retarded Green's function (GF) for the system,

$$G(\mathbf{r}, \mathbf{r}'; \omega) = \langle \mathbf{r} | (\omega - H + i0^+)^{-1} | \mathbf{r}' \rangle, \quad (11)$$

is computed from the Dyson equation

$$G(\mathbf{r}, \mathbf{r}'; \omega) = G_0(\mathbf{r}, \mathbf{r}'; \omega) + V_0 \int_C ds G_0(\mathbf{r}, \mathbf{R}(s); \omega) G(\mathbf{R}(s), \mathbf{r}'; \omega).$$

In this equation,  $G_0(\mathbf{r}, \mathbf{r}'; \omega)$  is the free-particle GF, i.e. the GF in the absence of the corral's wall, but in the presence of SOC,<sup>26,27</sup>

$$G_0(\mathbf{r}, \mathbf{r}'; \omega) = G_0^0(R; \omega) I + G_0^1(R; \omega) \begin{pmatrix} 0 & -ie^{-i\theta} \\ ie^{i\theta} & 0 \end{pmatrix}$$

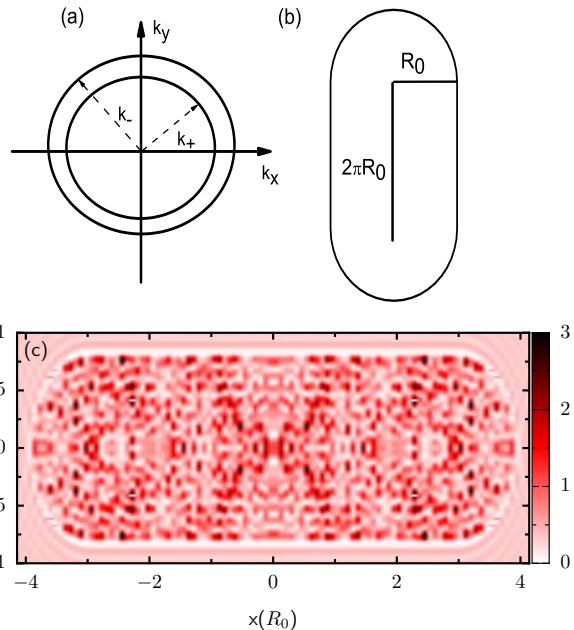


FIG. 3: (color online) (a) Spin-split energy surfaces with wave vectors  $k_+$  and  $k_-$ . (b) Stadium billiard considered in this work. (c) Spatial scan of the LDOS of a typical chaotic eigenfunction.

where

$$G_0^0(R; \omega) = -i \frac{m}{2k} \left\{ k_- H_0^{(1)}(Rk_-) + k_+ H_0^{(1)}(Rk_+) \right\},$$

$$G_0^1(R; \omega) = -\frac{m}{2k} \left\{ k_- H_1^{(1)}(Rk_-) - k_+ H_1^{(1)}(Rk_+) \right\}, \quad (12)$$

and  $\exp(i\theta) = [(x - x') + i(y - y')]/R$ , with  $H_0^{(1)}(x)$  and  $H_1^{(1)}(x)$  being Hankel functions,<sup>23</sup> with  $R=|\mathbf{r} - \mathbf{r}'|$  and  $k_{\pm}$  defined as before. The LDOS is then obtained from the GF via  $A(\mathbf{r}, \omega) = -(1/\pi) \text{Im Tr} [G(\mathbf{r}, \mathbf{r}; \omega)]$ .

The stadium billiard we consider is shown schematically in Fig. 3b. With energy in units of  $E_0=1/(2mR_0^2)$  and SOC in units of  $\alpha_0=1/(mR_0)$ , where  $R_0$  is the radius of the stadium's circular cap, we have considered eigenstates with energy  $E \simeq 405E_0$ , and have investigated SOCs in the range  $0 \leq \alpha \leq 10\alpha_0$ . [Choosing  $R_0=70\text{\AA}$ , and  $m=0.26m_e$  (with  $m_e$  being the electron's rest mass), one obtains  $\alpha_0=3.7 \times 10^{-11} \text{eVm}$ , a value consistent with e.g. electrons on an Au(111) surface.<sup>27,28</sup>] A spatial scan of the LDOS for a typical eigenstate considered is shown in Fig. 3c; from the LDOS, one- and two-point distribution functions were computed, going from the GOE to the GSE (with increasing  $\alpha$ ).

### IV. RESULTS

We now analyze the properties of the system, comparing results from RMT with those obtained by direct

simulation of Eq. 2 for a stadium billiard. We begin by determining the regimes which arise as function of the SOC strength. To this end, we consider the one-point function  $\mathcal{P}(\nu) = \langle \delta(\nu - A|\psi_\sigma(\mathbf{r})|^2) \rangle$ , which is obtained from Eq. 3 by integrating out the degrees of freedom except at  $\mathbf{r}$ . Using Eq. 5, we obtain

$$\begin{aligned} \mathcal{P}(\nu) &= \frac{\nu}{4\gamma_1\gamma_2\gamma_3\gamma_4} \int_0^1 dz \quad (13) \\ &\times \exp \left\{ -\frac{\nu}{4} \left[ (1-z) \left( \frac{1}{\gamma_1^2} + \frac{1}{\gamma_2^2} \right) + z \left( \frac{1}{\gamma_3^2} + \frac{1}{\gamma_4^2} \right) \right] \right\} \\ &\times I_0 \left[ \frac{\nu}{4} \left( \frac{1}{\gamma_1^2} - \frac{1}{\gamma_2^2} \right) (1-z) \right] I_0 \left[ \frac{\nu}{4} \left( \frac{1}{\gamma_3^2} - \frac{1}{\gamma_4^2} \right) z \right], \end{aligned}$$

where  $I_0(x)$  is the modified Bessel function of order-zero.<sup>23</sup> This expression reduces to  $\mathcal{P}_{\text{GOE}}(\nu) = \exp(-\nu/2)/\sqrt{2\pi\nu}$  in the GOE ( $\gamma_1=1$  and  $\{\gamma_i\}=0$  for  $i \neq 1$ ) and  $\mathcal{P}_{\text{GSE}}(\nu) = 4\nu \exp(-2\nu)$  in the GSE ( $\gamma_i=1/2 \forall i$ ).

Figure 4 shows numerical results for  $\mathcal{P}(\nu)$  for different values of the SOC; the results are compared with Eq. 13 in a “mean-field” description, i.e. with the  $\{\gamma_i\}$  evaluated at their average values — for  $\alpha=0.2\alpha_0$  ( $\alpha=0.5\alpha_0$ ), we find  $\lambda = 0.04\sqrt{4N}$  ( $\lambda = 0.08\sqrt{4N}$ ).<sup>29</sup> The physics of Eq. 2 is determined by its two length scales — the spin-flip length  $l_{\text{sf}}=1/(m\alpha)$  and the linear dimension of the system  $L$  ( $\simeq R_0$ ). Figure 4 shows how the system evolves toward the GSE as the SOC is increased. In particular, we find the system to be in the GSE for  $\alpha \gtrsim 1.5\alpha_0$  i.e.  $l_{\text{sf}} \lesssim 2R_0/3$ ; once the system is in this GSE regime, the statistics do not change further as the SOC is increased.

We now turn to spatial correlations of eigenfunctions. We first consider the amplitude correlator  $C_{\sigma\sigma'}(\mathbf{r}, \mathbf{r}') = \langle A|\psi_\sigma(\mathbf{r})|^2 A|\psi_{\sigma'}(\mathbf{r}')|^2 \rangle$ . Using the parameterization in

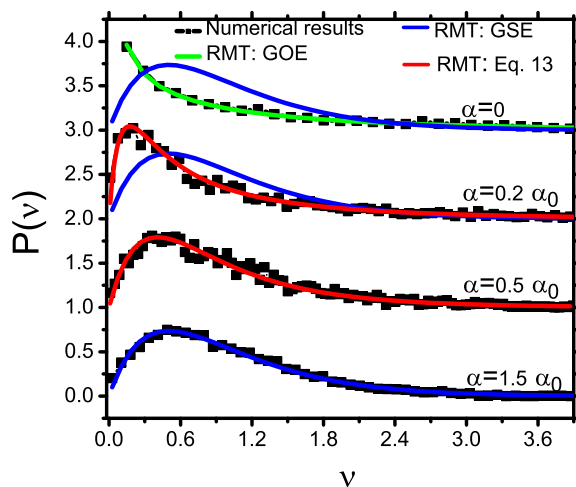


FIG. 4: (color online)  $\mathcal{P}(\nu) = \langle \delta(\nu - A|\psi_\sigma(\mathbf{r})|^2) \rangle$ . From top to bottom:  $\alpha=0$  (GOE),  $\alpha=0.2$ ,  $\alpha=0.5$ ,  $\alpha=1.5$  (GSE). Each curve has been vertically offset by one unit for clarity.

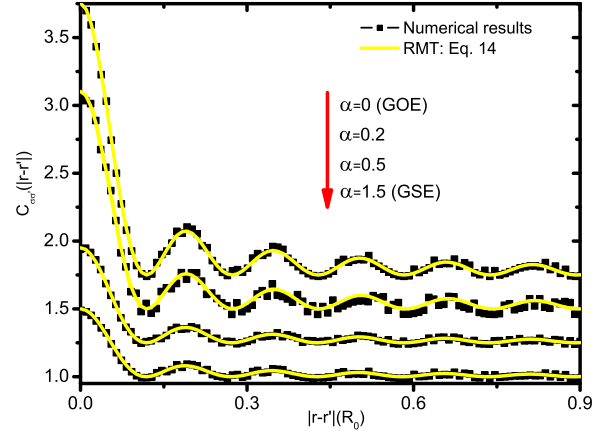


FIG. 5: (color online) Amplitude correlator  $C_{\sigma\sigma'}(\mathbf{r}, \mathbf{r}') = \langle A|\psi_\sigma(\mathbf{r})|^2 A|\psi_{\sigma'}(\mathbf{r}')|^2 \rangle$ . From top to bottom:  $\alpha=0$  (GOE),  $\alpha=0.2\alpha_0$ ,  $\alpha=0.5\alpha_0$ ,  $\alpha=1.5\alpha_0$  (GSE). Each curve has been vertically offset by  $1/4$  unit for clarity.

Eq. 5, we obtain

$$\begin{aligned} C_{\sigma\sigma'}(\mathbf{r}, \mathbf{r}') &= 1 + 2 \left[ (\gamma_1^4 + \gamma_2^4 + \gamma_3^4 + \gamma_4^4) f^2 \right. \\ &\quad \left. + 2(\gamma_1^2\gamma_3^2 + \gamma_2^2\gamma_4^2) g^2 \right]. \quad (14) \end{aligned}$$

Notice that this reduces to  $C_{\sigma\sigma'}^{\text{GOE}}(\mathbf{r}, \mathbf{r}') = 1 + 2f^2$  in the GOE, and to  $C_{\sigma\sigma'}^{\text{GSE}}(\mathbf{r}, \mathbf{r}') = 1 + \mathcal{V}^2/2$  in the GSE where  $\mathcal{V}^2=f^2+g^2$ . Numerical results for  $C_{\sigma\sigma'}(\mathbf{r}, \mathbf{r}')$  are shown in Fig. 5 and are compared with Eq. 14, with the  $\{\gamma_i\}$  evaluated at their average values (as before). We see that the maximum is larger in the GOE; more generally, the correlations decay more rapidly with SOC — amplitude correlations are suppressed as  $\sigma$ -invariance is broken.

Having determined the parameter regimes and, in particular, how large the SOC must be to be in the GSE, we now consider in greater detail the properties of the system in the GSE. To this end, we consider the joint distribution function  $\mathcal{P}(\nu_1, \nu_2) = \langle \delta(\nu_1 - A|\psi_\sigma(\mathbf{r})|^2) \delta(\nu_2 - A|\psi_{\sigma'}(\mathbf{r}')|^2) \rangle$ , which is obtained from Eq. 3 by integrating out the degrees of freedom except those at  $\mathbf{r}$  and  $\mathbf{r}'$ . For the GSE we obtain

$$\mathcal{P}_{\text{GSE}}(\nu_1, \nu_2) = \frac{8\sqrt{\nu_1\nu_2}}{\mathcal{V}(1-\mathcal{V}^2)} \exp(-2\mathcal{X}_S) I_1(4\mathcal{X}_P), \quad (15)$$

where  $I_1(x)$  is the modified Bessel function of order-1;<sup>23</sup> for comparison, we also consider  $\mathcal{P}(\nu_1, \nu_2)$  in the GOE<sup>18</sup>

$$\mathcal{P}_{\text{GOE}}(\nu_1, \nu_2) = \frac{\exp(-\mathcal{X}_S/2) \cosh(\mathcal{X}_P)}{2\pi\sqrt{1-f^2}\sqrt{\nu_1\nu_2}}.$$

In the above equations,  $\mathcal{X}_S=(\nu_1 + \nu_2)/(1 - \mathcal{X}^2)$  and  $\mathcal{X}_P=\mathcal{X}\sqrt{\nu_1\nu_2}/(1 - \mathcal{X}^2)$  where  $\mathcal{X}=\mathcal{V}$  ( $\mathcal{X}=f$ ) for the GSE (GOE).

We now consider the properties and consequences of  $\mathcal{P}(\nu_1, \nu_2)$ . We begin by considering the conditional probability

$$\mathcal{P}_{\nu_1}(\nu_2) = \mathcal{P}(\nu_1, \nu_2)/\mathcal{P}(\nu_1) \quad (16)$$

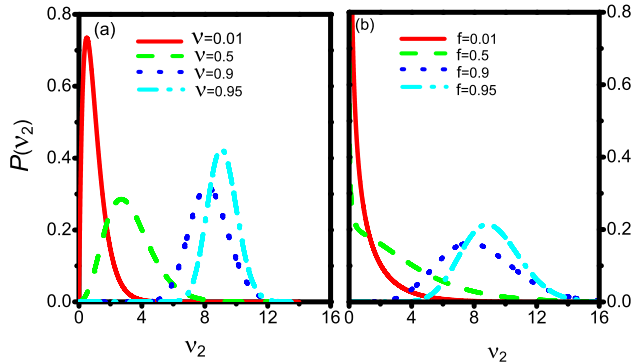


FIG. 6: (color online) Conditional probability (a)  $\mathcal{P}_{\nu_1}^{\text{GSE}}(\nu_2)$ , and (b)  $\mathcal{P}_{\nu_1}^{\text{GOE}}(\nu_2)$ , for several values of  $\mathcal{V}$  ( $f$ ), for  $\nu_1 = 10$ .

which describes the wave function distribution at  $\mathbf{r}_2$ , provided  $A|\psi(\mathbf{r}_1)|^2 = \nu_1$ . It follows from Eq. 16 that correlations between fluctuations at different points depend on their amplitudes<sup>30</sup> — regions of high amplitude (i.e. large  $\nu_1$ ) are correlated over larger distances, while regions of small amplitude are correlated over shorter distances.  $\mathcal{P}_{\nu_1}^{\text{GSE}}(\nu_2)$  for the GSE is shown in Fig. 6a for several values of  $\mathcal{V} = \sqrt{f^2 + g^2}$ ;  $\mathcal{P}_{\nu_1}^{\text{GOE}}(\nu_2)$  for the GOE is shown in Fig. 6b for comparison, for several values of  $f$ .

From Eq. 16, one can obtain the average  $\langle \nu_2 \rangle_{\nu_1}$  and the mean squared fluctuation  $\langle (\delta \nu_2)^2 \rangle_{\nu_1} = \langle \nu_2^2 \rangle_{\nu_1} - \langle \nu_2 \rangle_{\nu_1}^2$ , where  $\langle \dots \rangle_{\nu_1}$  denotes an average with respect to  $\mathcal{P}_{\nu_1}(\nu_2)$ :

$$\begin{aligned} \langle \nu_2 \rangle_{\nu_1} &= 1 + \mathcal{X}^2(\nu_1 - 1), \\ \langle (\delta \nu_2)^2 \rangle_{\nu_1} &= \mathcal{C} [1 + 2\mathcal{X}^2(\nu_1 - 1) + \mathcal{X}^4(1 - 2\nu_1)], \end{aligned} \quad (17)$$

where  $\mathcal{C}=2$  for the GOE,<sup>12</sup> while  $\mathcal{C}=1/2$  for the GSE. [As before,  $\mathcal{X}=\mathcal{V}(f)$  for the GSE (GOE).] From this, we see that fluctuations are suppressed in the GSE compared to the GOE. More generally, fluctuations are largest in the GOE (compared with the GUE<sup>30</sup> and the GSE, Eq. 17) and, hence, correlations are the weakest.

We now consider the distribution of the product  $A|\psi_\sigma(\mathbf{r})\psi_{\sigma'}(\mathbf{r}')|$ ,  $\mathcal{P}(\Gamma) = \langle \delta(\Gamma - A|\psi_\sigma(\mathbf{r})\psi_{\sigma'}(\mathbf{r}')|) \rangle$ .  $\mathcal{P}(\Gamma)$  determines a number of experimentally relevant quantities, such as the form factor in resonant scattering in complex nuclei,<sup>11</sup> amplitudes in tunneling measurements, and the conductance amplitude distribution through small quantum dots.<sup>9</sup> From Eq. 15, we obtain for the GSE

$$\mathcal{P}_{\text{GSE}}(\Gamma) = \frac{32 \Gamma^2}{|\mathcal{V}|(1 - \mathcal{V}^2)} I_1 \left( \frac{4|\mathcal{V}| \Gamma}{1 - \mathcal{V}^2} \right) K_0 \left( \frac{4 \Gamma}{1 - \mathcal{V}^2} \right), \quad (18)$$

where  $K_0(x)$  is a modified Bessel function of order zero;<sup>23</sup> in the GOE, we obtain

$$\mathcal{P}_{\text{GOE}}(\Gamma) = \frac{2}{\pi \sqrt{1 - f^2}} K_0 \left( \frac{\Gamma}{1 - f^2} \right) \cosh \left( \frac{f \Gamma}{1 - f^2} \right).$$

Figure 7 shows results for  $\mathcal{P}(\Gamma)$  for several values of  $\mathcal{V}$  ( $f$ ) for the GSE (GOE). We see that the maximum of

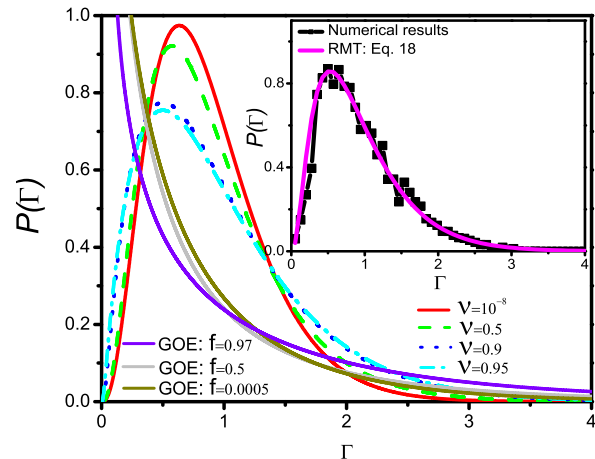


FIG. 7: (color online) Product distribution  $\mathcal{P}(\Gamma) = \langle \delta(\Gamma - A|\psi_\sigma(\mathbf{r})\psi_{\sigma'}(\mathbf{r}')|) \rangle$  in the GSE for several values of  $\mathcal{V}$ . For comparison,  $\mathcal{P}_{\text{GOE}}(\Gamma)$  is also shown for  $f = 0.5$ . Inset: Comparison of numerical and RMT results for  $R = 0.055R_0$ .

$\mathcal{P}_{\text{GSE}}(\Gamma)$  decreases with increasing  $\mathcal{V}$  with the tail becoming slightly longer. For comparison,  $\mathcal{P}_{\text{GOE}}(\Gamma)$  is shown for different values of  $f$ . We see that correlations play a more significant role in the GSE — indeed, except for a very small region near  $\Gamma=0$ ,  $\mathcal{P}_{\text{GOE}}(\Gamma)$  is essentially indistinguishable from the result with  $f \rightarrow 0$ . This is a consequence of the fact that fluctuations are largest in the GOE and correlations are the weakest. Shown in the inset are numerical results for  $\mathcal{P}_{\text{GSE}}(\Gamma)$  for  $R=0.055R_0$  in comparison with the RMT result, Eq. 18.

## V. CONCLUDING REMARKS

To summarize, we have investigated the statistical properties of wave functions in (two-dimensional) chaotic nanostructures with spin-orbit interactions, focussing particularly on spatial correlations of eigenfunctions. Numerical results obtained for a chaotic stadium billiard were compared with (analytic) results from RMT. It was found that excellent agreement between RMT and microscopic simulations are obtained in a “mean-field” description of the GOE-GSE crossover. A key observation from our results is that correlations of wave function amplitudes are suppressed with SOC. Interestingly, however, these correlations with SOC play a more significant role in the two-point distribution function(s).

Our results have implications for a number of systems of current interest. Indeed, the effects of SOC have been observed in transport through quantum dots.<sup>31</sup> These effects could also be observed in quantum corrals defined on Au and Ag (111) surfaces,<sup>27</sup> where large SOC has been observed recently,<sup>32</sup> especially as scanning tunneling microscopy techniques have exquisite control of positioning and correlation measurements.

### Acknowledgements

We acknowledge helpful conversations with H. U. Baranger and P. W. Brouwer. EHK acknowledges the

warm hospitality of the Instituto de Física Teórica (Madrid), where most of this work was performed. This work was supported in Ohio by NSF-DMR MWN/CIAM and NSF-PIRE grants.

- 
- <sup>1</sup> See, e.g. K. C. Nowack, F. H. L. Koppens, Yu. V. Nazarov, and L. M. K. Vandersypen, *Science* **318**, 1430 (2007), and references therein.
- <sup>2</sup> Y. Alhassid, *Rev. Mod. Phys.* **72**, 895 (2000).
- <sup>3</sup> For a review, see e.g. M. C. Daniel and D. Astruc, *Chem Rev* **104**, 293 (2004).
- <sup>4</sup> See e.g., E. J. Heller, *Nature Phys.* **4**, 443 (2008).
- <sup>5</sup> M. L. Mehta, *Random Matrices* (Elsevier, San Diego, 2004).
- <sup>6</sup> F. Haake, *Quantum Signatures of Chaos*, 3rd ed. (Springer, Berlin, 2010).
- <sup>7</sup> A. M. Chang, H. U. Baranger, L. N. Pfeiffer, K. W. West, and T. Y. Chang, *Phys. Rev. Lett.* **76**, 1695 (1996); J. A. Folk, S. R. Patel, S. F. Godijn, A. G. Huibers, S. M. Cronenwett, and C. M. Marcus, *Phys. Rev. Lett.* **76**, 1699 (1996).
- <sup>8</sup> Y. Alhassid and C. H. Lewenkopf, *Phys. Rev. Lett.* **75**, 3922 (1995).
- <sup>9</sup> V. N. Prigodin, K. B. Efetov, and S. Iida, *Phys. Rev. Lett.* **71**, 1230 (1993).
- <sup>10</sup> J. B. French, V. K. B. Kota, A. Pandey, and S. Tomsovic, *Ann. Phys.* **181**, 198 (1988).
- <sup>11</sup> J. J. M. Verbaarschot, H. A. Weidenmüller, and M. R. Zirnbauer, *Phys. Rep.* **129**, 367 (1985).
- <sup>12</sup> V. N. Prigodin, N. Taniguchi, A. Kudrolli, V. Kidambi, and S. Sridhar, *Phys. Rev. Lett.* **75**, 2392 (1995).
- <sup>13</sup> C. Gmachl, F. Capasso, E. E. Narimanov, J. U. Nockel, A. D. Stone, J. Faist, D. L. Sivco, A. Y. Cho, *Science* **280**, 1556 (1998); J. U. Nockel, A. D. Stone, G. Chen, H. L. Grossman, and R. K. Chang, *Optics Lett.* **21**, 1609 (1996).
- <sup>14</sup> V. Doya, O. Legrand, and F. Mortessagne, *Optics Lett.* **26**, 872 (2001).
- <sup>15</sup> K. A. Matveev, L. I. Glazman, and A. I. Larkin, *Phys. Rev. Lett.* **85**, 2789 (2000); P. W. Brouwer, X. Waintal, and B. I. Halperin, *Phys. Rev. Lett.* **85**, 369 (2000).
- <sup>16</sup> E. N. Bulgakov and A. F. Sadreev, *JETP Lett.* **78**, 443 (2003); Y. Alhassid and T. Rupp, cond-mat/0312691; G. Murthy and R. Shankar, *Phys. Rev. B* **75**, 075327 (2007); O. Zelyak and G. Murthy, *Phys. Rev. B* **80**, 205310 (2009).
- <sup>17</sup> L. A. Bunimovich, *Funct. Anal. Appl.* **8**, 254 (1974); *Commun. Math. Phys.* **65**, 295 (1979).
- <sup>18</sup> M. Srednicki, *Phys. Rev. E* **54**, 954 (1996).
- <sup>19</sup> J. D. Urbina and K. Richter, *Phys. Rev. Lett.* **97**, 214101 (2006); *Phys. Rev. E* **70**, 015201(R) (2004).
- <sup>20</sup> S. Adam, M. L. Polianski, X. Waintal, and P. W. Brouwer, *Phys. Rev. B* **66**, 195412 (2002).
- <sup>21</sup> Y. Alhassid, J. N. Hormuzdiar, and N. D. Whelan, *Phys. Rev. B* **58**, 4866 (1998).
- <sup>22</sup> Eqs. 8a and 8b were computed in an approximation which assumes translation invariance; this is known to give reasonable results away from the boundaries.
- <sup>23</sup> I. S. Gradshteyn and I. M. Ryzhik, *Table of Integrals, Series, and Products* (Academic Press, San Diego 1994).
- <sup>24</sup> M. V. Berry, *J. Phys. A* **10**, 2083 (1977).
- <sup>25</sup> M. G. E. Luz, A. S. Lupu-Sax, and E. J. Heller, *Phys. Rev. E* **56**, 2496 (1997).
- <sup>26</sup> H. Imamura, P. Bruno, and Y. Utsumi, *Phys. Rev. B* **69**, 121303(R) (2004).
- <sup>27</sup> J. D. Walls and E. J. Heller, *Nano Lett.* **7**, 3377 (2007).
- <sup>28</sup> J. Henk, A. Ernst, and P. Bruno, *Phys. Rev. B* **68**, 165416 (2003); S. LaShell, B. A. Dougall, and E. Jensen, *Phys. Rev. Lett.* **77**, 3419 (1996).
- <sup>29</sup>  $\lambda$  (in Eq. 1) was determined by minimizing the  $\chi^2$  deviation between Eq. 13 and the numerical data.
- <sup>30</sup> V. N. Prigodin, *Phys. Rev. Lett.* **74**, 1566 (1995).
- <sup>31</sup> J. B. Miller, D. M. Zumbühl, C. M. Marcus, Y. B. Lyanda-Geller, D. Goldhaber-Gordon, K. Campman, and A. C. Gossard, *Phys. Rev. Lett.* **90**, 076807 (2003).
- <sup>32</sup> G. Nicolay, F. Reinert, and S. Hufner, and P. Blaha, *Phys. Rev. B* **65**, 033407 (2001).

